



This is a repository copy of *Hydrogen Tunneling Above Room Temperature Evidenced by Infrared Ion Spectroscopy*.

White Rose Research Online URL for this paper:
<http://eprints.whiterose.ac.uk/113539/>

Version: Accepted Version

Article:

Schäfer, M., Peckelsen, K., Paul, M. et al. (5 more authors) (2017) Hydrogen Tunneling Above Room Temperature Evidenced by Infrared Ion Spectroscopy. *Journal of the American Chemical Society*. ISSN 0002-7863

<https://doi.org/10.1021/jacs.6b10348>

Reuse

Unless indicated otherwise, fulltext items are protected by copyright with all rights reserved. The copyright exception in section 29 of the Copyright, Designs and Patents Act 1988 allows the making of a single copy solely for the purpose of non-commercial research or private study within the limits of fair dealing. The publisher or other rights-holder may allow further reproduction and re-use of this version - refer to the White Rose Research Online record for this item. Where records identify the publisher as the copyright holder, users can verify any specific terms of use on the publisher's website.

Takedown

If you consider content in White Rose Research Online to be in breach of UK law, please notify us by emailing eprints@whiterose.ac.uk including the URL of the record and the reason for the withdrawal request.



eprints@whiterose.ac.uk
<https://eprints.whiterose.ac.uk/>

Hydrogen Tunneling Above Room Temperature Evidenced by Infrared Ion Spectroscopy

Mathias Schäfer^{†*}, Katrin Peckelsen[†], Mathias Paul[†], Jonathan Martens[‡], Jos Oomens^{‡,§*}, Giel Berden[‡], Albrecht Berkessel^{†*}, and Anthony J. H. M. Meijer^{||*}

[†]Department of Chemistry, Organic Chemistry, University of Cologne, Greinstraße 4, 50939 Cologne, Germany.

[‡]Radboud University, Institute for Molecules and Materials, FELIX Laboratory, Toernooiveld 7c, 6525 ED Nijmegen, The Netherlands.

[§]*van 't Hoff Institute for Molecular Sciences, University of Amsterdam, Science Park 904, 1098 XH Amsterdam, The Netherlands.*

^{||}Department of Chemistry, University of Sheffield, Sheffield S3 7HF, UK.

KEYWORDS: carbenes; tunneling; mass spectrometry; infrared ion spectroscopy; DFT calculations

ABSTRACT: While hydrogen tunneling at elevated temperatures has, for instance, often been postulated in biochemical processes, spectroscopic proof is thus far limited to cryogenic conditions, under which thermal reactivity is negligible. We report spectroscopic evidence for H-tunneling in the gas phase at temperatures around 320-350K observed in the isomerization reaction of a hydroxycarbene into an aldehyde. The charge-tagged carbene was generated in situ in a tandem mass spectrometer by decarboxylation of oxo[4-(trimethylammonio)phenyl]acetic acid upon collision induced dissociation. All ion structures involved are characterized by infrared ion spectroscopy and quantum chemical calculations. The charge-tagged phenylhydroxycarbene undergoes 1,2-H-shift to the corresponding aldehyde with a half-life of about 10 s, evidenced by isomer-selective two-color (IR-IR) spectroscopy. In contrast, the deuterated (OD) carbene analogue showed much reduced 1,2-D-shift reactivity with an estimated half-life of at least 200 seconds under the experimental conditions, and provides clear evidence for hydrogen atom tunneling in the H-isotopologue. This is the first spectroscopic confirmation of hydrogen atom tunneling governing 1,2-H-shift reactions at non-cryogenic temperatures, which is of broad significance for a range of (bio)chemical processes, including enzymatic transformations and organocatalysis.

I. INTRODUCTION

Rates and selectivities of chemical reactions are classically defined by energy barriers, but can be significantly biased by quantum-mechanical tunneling.^{1,2} Indeed, hydrogen tunneling is known to play a crucial role in chemical reactivity at cryogenic temperatures, such as in astrochemistry, and at room temperature in biochemistry, organic chemistry, and catalysis. However, the effect of tunneling processes at room temperature are, until now, mainly recognized on the basis of kinetic isotopic effect measurements^{3,4} and direct spectroscopic proof for tunneling control of chemical reactions is thus far limited to cryogenic conditions, where thermal reactivity is negligible.⁵⁻¹⁰

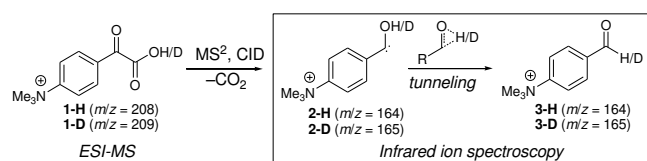
From 2008 onwards, Schreiner and Allen et al. have demonstrated that α -ketocarboxylic acids such as glyoxylic acid, phenylglyoxylic and pyruvic acid, can be decarboxylated by flash-vacuum pyrolysis to form the

respective hydroxycarbenes. Characterization of the trapped hydroxycarbenes by infrared (IR) spectroscopy in an argon matrix at 11 K,⁶⁻⁸ in combination with high-level computations, established that the isomerization of hydroxycarbenes to their respective aldehydes and enols, proceeds by a tunneling controlled 1,2-hydrogen shift reaction. This conclusion is consistent with the predominant formation of the thermodynamic product through hydrogen tunneling under the higher kinetic barrier at cryogenic temperatures.⁶⁻⁹

In addition, O'Hair demonstrated in his extensive work on the fundamentals of the Pesci decarboxylation reaction¹¹ that charged carboxylate metal complexes expel neutral CO₂ to form metal-ion carbene complexes upon collision induced dissociation (CID) in the gas phase of a mass spectrometer (MS). The tandem MS experiments were conducted at room temperature in a linear quadrupole ion trap (QIT) with subsequent structure analysis of the organometallic ions by UV ion

spectroscopy. Furthermore, this set-up allows investigations of the intrinsic reactivity of the in situ formed analytes via ion–molecule reactions (IMR). To investigate the decarboxylation reaction of α -ketocarboxylic acids, which is of central importance for e.g. thiamine dependent enzyme catalysis with pyruvate decarboxylases,¹² we synthesized a charge-tagged phenylglyoxylic acid derivative. As illustrated in Scheme 1, the fixed-charge α -ketocarboxylic acid precursor ions are transferred into the gas-phase by electrospray ionization (ESI) for analysis in a QIT mass spectrometer.¹³

Scheme 1. Gas-phase formation of a hydroxycarbene from an α -ketocarboxylic acid precursor in a QIT at room temperature.



The molecular ions of oxo[4-(trimethylammonio)phenyl]acetic acid (**1-H** at m/z 208) and its mono-deuterated derivative (**1-D** at m/z 209) are selected and dissociated by collisional activation. The loss of CO_2 via CID delivers a pair of isobaric product ions (**2-H**, **3-H** at m/z 164 from precursor **1-H**, and **2-D**, **3-D** at m/z 165 from **1-D**, respectively) in a charge-remote fragmentation process.¹⁴ Samples of 4-(trimethylammonio)benzaldehyde (**3-H**) and its isotopomer **3-D** were also prepared and characterized spectroscopically as reference data sets for comparison (see SI for details). For the identification and characterization of individual isomers in a mixture of isobaric product ions, i.e. the charge-tagged hydroxycarbene **2-H** and the respective aldehyde **3-H**, and isotopologues **2-D** and **3-D**, we used infrared ion spectroscopy.¹⁵ Wavelength-tunable radiation from a free electron laser (FEL) and optical parametric oscillator (OPO) laser sources was used for the irradiation of ions stored in a spherical QIT mass spectrometer.¹³ As the density of ions stored in a QIT is far too low for direct IR absorption spectroscopy, the extent of precursor ion depletion and product ion formation is monitored as the energy of the photons used for activation is tuned (FEL: from 600 to 1800 cm^{-1} and OPO: 2500-3700 cm^{-1}). In infrared ion spectroscopy, the energy of tens to hundreds of resonantly absorbed photons is turned into vibrational excitation of all oscillators of the activated ion due to intramolecular vibrational redistribution (IVR), which ultimately leads to internal energies where one or more dissociation pathways become accessible. Infrared ion spectroscopy combined with a computational analysis of ion structures has proven to be a powerful analytical strategy to elucidate ion structures.¹⁵

II. RESULTS AND DISCUSSION

II.1 Characterization of hydroxy[4-(trimethylammonio)phenyl]carbene (**2-H**) by infrared ion spectroscopy and theory

Decarboxylation of **1-H/1-D** can result in both **2-H/2-D** and **3-H/3-D** product ions (m/z 164/165) which have been characterized here by infrared ion spectroscopy.^{13, 15} The infrared ion spectra of the isobaric product ions **2-H/3-H** at m/z 164 (Figure 1 a-c), and of **2-D/3-D** at m/z 165 (Supplementary Figure 6a and 6c), result from the monitoring of the depletion of the respective precursor ion and their photo-fragment ions upon IRMPD. The predominant fragmentation process in all cases is the loss of a methyl radical, along with the loss of C_2H_4 and CH_4 and combinations of these (see Supplementary Table 3, SI for details). These results are presented in Fig. 1 in which panel (a) displays the infrared spectrum (black) of product ions isolated at m/z 164 compared to the computed IR spectrum of the singlet trans-hydroxycarbene, **2-H_t** (see Supplementary Fig. 3 for comparison of the computed IR spectrum of the singlet cis-hydroxycarbene, **2-H_c**). The presence of **2-H_t** in the ion population at m/z 164 is immediately identified by the presence of an OH stretching vibration, $\nu_{\text{O-H}}$, at 3553 cm^{-1} and a C-O stretch mode $\nu_{\text{C-O}}$ at 1248 cm^{-1} , both matching the calculated bands for **2-H_t**. In panel (b), the experimental (black) and calculated (red) IR spectra of the synthesized aldehyde **3-H** model compound (4-(trimethylammonio)benzaldehyde) are presented, showing an absence of intensity in the region of 1250 cm^{-1} and between 3500-3600 cm^{-1} where the $\nu_{\text{O-H}}$ and $\nu_{\text{C-O}}$ resonances are found for the hydroxycarbene **2-H_t**. As well, the characteristic aldehyde $\nu_{\text{C=O}}$ stretch for **3-H** above 1700 cm^{-1} in panel (b) identifies the corresponding band at the same position in the experimental spectrum in panel (a), unaccounted for the calculated IR spectrum of **2-H_t**. This clearly indicates a mixture of **2-H_t** and **3-H** in the ion population at m/z 164 (see Supplementary Fig. 4 for comparison with other constitutional isomers and Supplementary Table 1).⁸ A horizontal dashed line in panel (b) indicates a threshold below which IR resonances are of insufficient intensity to absorb the required number of photons to reach the dissociation limit of the molecule, so that these resonances remain unobserved in the experimental spectrum. While this threshold limits the number of bands observed experimentally for the aldehyde species (in both panels (b) and (c) of Fig. 1.), we see that this is not the case for the hydroxycarbene resonances in panel (a), where most of even the weakest bands still appear in the experimental spectrum. This apparent lower dissociation threshold of the hydroxycarbene **2-H_t** is attributed to isomerization of the hydroxycarbene to the aldehyde during IR photodissociation measurements, where the energy released by

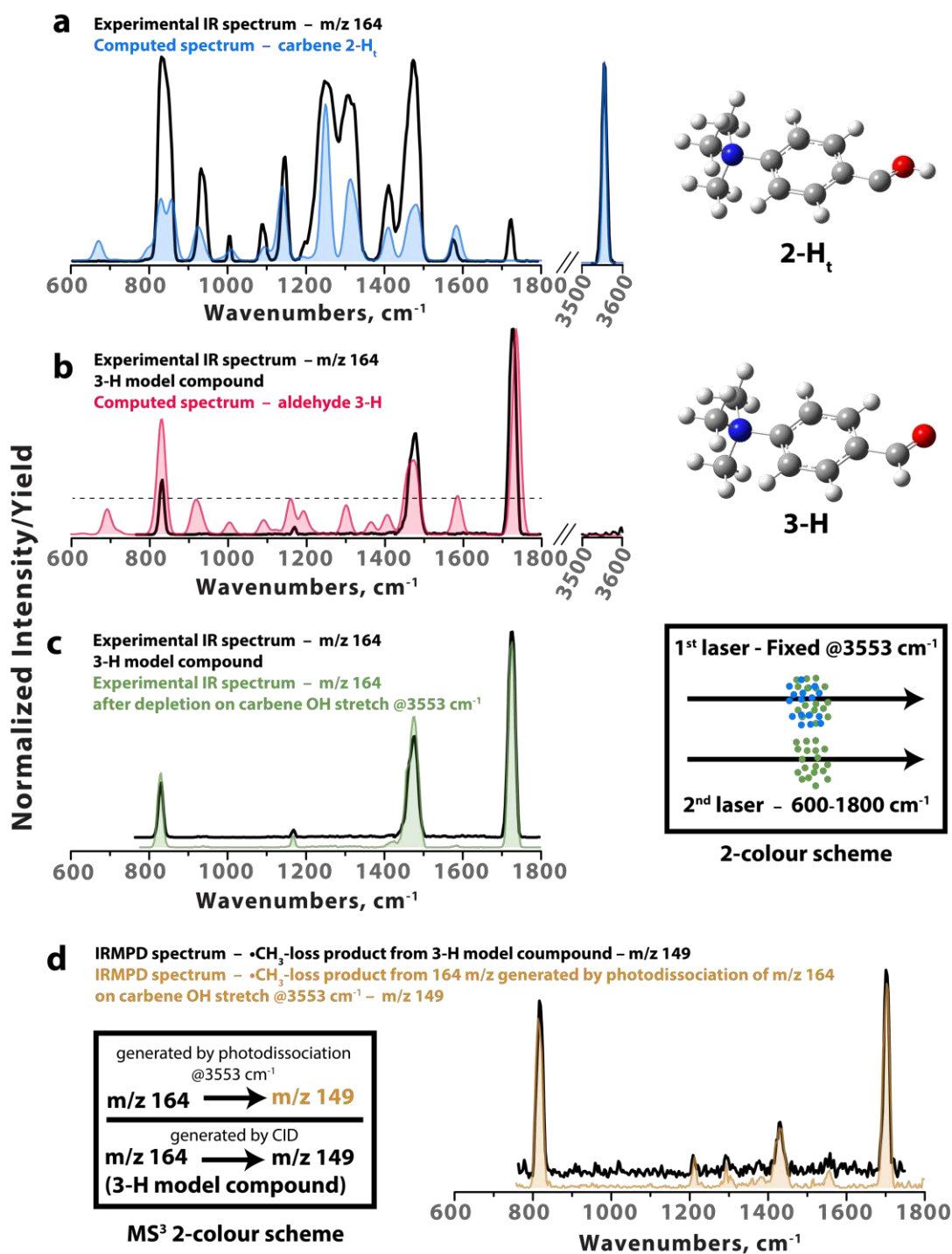


Figure 1. Experimental and calculated infrared spectra. (a) The experimental IR spectrum of the ion population at m/z 164 generated by CO₂ loss from 1-H (black; see Supplementary Table 3; SI) is compared to the calculated IR spectrum of the charge-tagged trans-hydroxycarbene, 2-H_t (blue). (b) The experimental IR spectrum of the synthesized aldehyde (4-(trimethylammonio)benzaldehyde) model compound (black; see Supplementary Table 3; SI) is compared with the calculated IR spectrum (red) for 3-H. (c) The experimental IR spectrum (green) of the remaining ions at m/z 164 in an isomer-selective two-colour IR-IR experiment (see (c) inset) is compared to the experimental IR spectrum of reference compound 3-H. (d) The experimental IR spectrum of the •CH₃ loss product (m/z 149) recorded after isomer-selective photodissociation of hydroxycarbene 2-H_t species is compared to the experimental IR spectrum of the CID generated •CH₃ loss product (m/z 149) from the 3-H model compound. The structures of 2-H_t and 3-H shown in the right of panels (a) and (b) have been computed at the dispersion-corrected B3LYP-GD3BJ/cc-pVTZ level of theory. Frequencies are scaled by 0.97 (500-2000 cm⁻¹)¹⁵ and by 0.95 (2800-3800 cm⁻¹).¹⁶

isomerization assists the system in reaching its dissociation threshold (fewer photons must be absorbed). Panel (c) of Fig. 1 presents an isomer-selective IR spectrum (green) of the aldehyde **3-H** component of the ion population at m/z 164. This spectrum is generated in a novel two-colour IR-IR approach. Here, the ion population at m/z 164 is first irradiated at 3553 cm^{-1} using a 10W cw-OPO source. At this frequency only the hydroxycarbene isomer is resonant ($\nu_{\text{O-H}}$), but the aldehyde is transparent. Hence, we selectively photo-dissociate the hydroxycarbene **2-H_t** ions in the population.⁸ In a second step, the remaining ions at m/z 164, those without a $\nu_{\text{O-H}}$ resonance at 3553 cm^{-1} , are re-isolated and probed with tuneable IR light to measure their infrared spectrum. The clear match between this isomer-selective IR spectrum and the reference spectrum measured for the **3-H** model compound (black, panels (b) and (c) of Fig. 1) confirms the assignment of **3-H** as the only additional component besides **2-H_t** of the ion population at m/z 164.

Panel (d) of Fig. 1 presents a second two-color IR-IR experiment where the IR spectrum of the photofragment at m/z 149, generated selectively from the hydroxycarbene (orange), is presented (see experimental section for details). Similar to the two-color approach in panel (b), hydroxycarbene ions at m/z 164 are first selectively photodissociated by irradiation at 3553 cm^{-1} . However, in the second step, rather than re-isolating the remaining ions at m/z 164, fragment ions at m/z 149 ($\bullet\text{CH}_3$ loss) are isolated and probed using tuneable IR light to generate their IR spectrum. The resulting spectrum features a sharp band at 1700 cm^{-1} , indicative of a $\nu_{\text{C=O}}$ stretch, strongly favoring the assignment of an aldehyde structure and not a hydroxycarbene structure. Additionally, the IR spectrum of the $\bullet\text{CH}_3$ loss product (m/z 149) from the **3-H** aldehyde model compound was measured (black) and matches very closely with the m/z 149 fragment generated selectively from the hydroxycarbene. Supplementary Fig. 5 (Supporting Information) presents calculated spectra for the $\bullet\text{CH}_3$ loss product from **2-H_t** and **3-H**, clearly demonstrating that the orange spectrum in panel (d) cannot be accounted for by a fragment ion with a hydroxycarbene structure (**7-H_t**), but matches well with the calculated IR spectrum of the corresponding, and energetically favored, aldehyde fragment (**6-H**). These observations directly implicate isomerization of the hydroxycarbene **2-H_t**, to the aldehyde **3-H**, during IR photodissociation. Our calculations also show that the energy needed to form **7-H_t** from **2-H_t** and to form **6-H** from **3-H** are 125.8 kJ mol^{-1} and 220.3 kJ mol^{-1} , respectively. These results are in agreement with the higher stability for **3-H** found in the experiment.

To further explore the energetics and pathways for the formation and reactions of the hydroxycarbene **2-H_t** and the aldehyde **3-H**, the zero-point corrected reaction energy profiles are presented in Figure 2. The corresponding Gibbs energy reaction profiles are given in Supplementary Figs. 9 and 10.

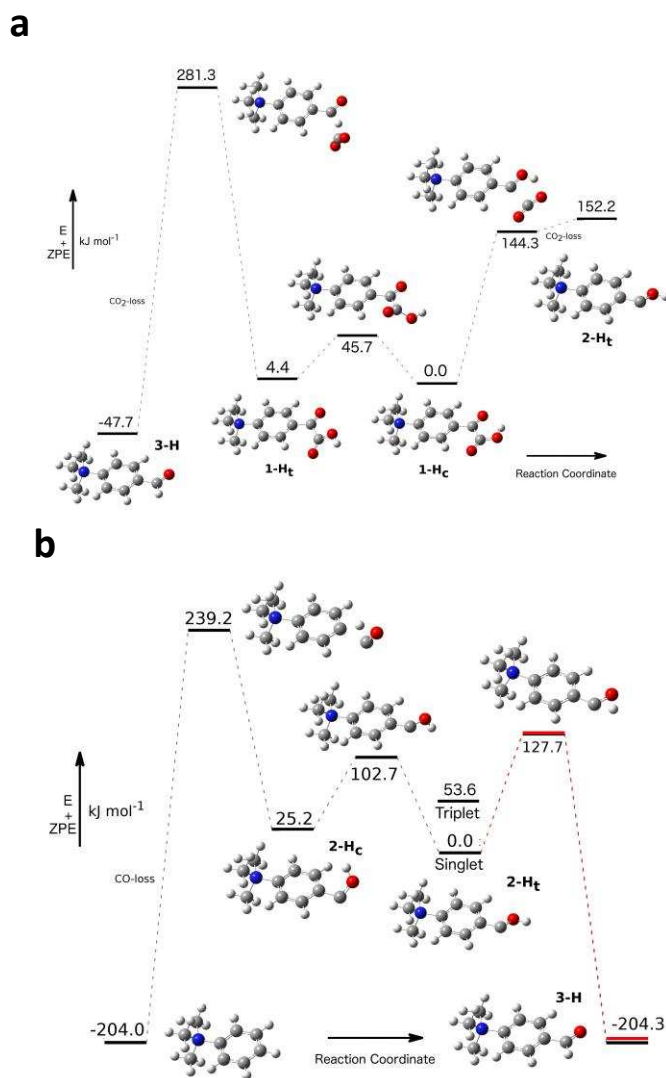


Figure 2. Reaction energy profiles.[§] (a) Formation of **2-H_t** from **1-H_c**, and **3-H** from **1-H_t**. (b) Conversion of **2-H_t** into **3-H** as well as for the CO -loss reaction from **2-H_c**, respectively. All structures have been calculated at the dispersion-corrected B3LYP-GD3BJ/cc-pVTZ level of theory. The red line indicates the corresponding zero-point corrected CCSD(T)-F12b energies. Reaction Gibbs free energy profiles are provided in Supplementary Figs. 9 and 10.

Figure 2 matches closely to the zero-point corrected CCSD(T) energies calculated by Schreiner and Allen et

[§] We have chosen to focus on single-molecule events here and are therefore plotting the internal energy. This allows for comparison with the internal energies used for the low temperature ($T=10\text{K}$) experiments of Schreiner et al.⁸ where all molecules will most likely be in a single quantum state.¹⁹ If we were to consider that in the trap the ions will be in a thermalized (above room temperature) distribution over quantum states before, during, and after the CID and IRMPD processes^{18a,18b} then the reaction profiles for the Gibbs energy from the SI are appropriate.

al. for phenylhydroxycarbene in terms of relative energies, multiplicity and transition states⁸ and demonstrate that the charge-tag does not significantly influence the energy profiles for **2-H_t** and **3-H**.¹⁷ As well, CCSD(T)-F12b calculations (see SI for details) on **2-H_t**, **3-H** and the barrier between them, as well as on the neutral analogues, confirm the validity of the DFT calculations (see also Supplementary Table 2). Panel (a) of Fig. 2 furthermore shows that **1-H** exists as two nearly isoenergetic conformers, **1-H_c** (cis) and **1-H_t** (trans), the latter of which is also found in the crystal structure of [4-(dimethylamino)phenyl]oxoacetic acid (**S-2-H**, see Supplementary Figs. 11 and 12 for overlays of structures).

The energy profiles in Fig. 2 indicate that the energy needed to form **2-H_t** is significantly less than the energy barrier for forming the aldehyde **3-H** (see Supplementary Table 2). Nevertheless, the aldehyde tautomer (**3-H**) is formed and experimentally identified as shown in Fig. 1 and discussed above. While the initial formation of the hydroxycarbene product ion **2-H_t** from precursor ion **1-H_t** is clearly favored as shown in panel (a) of Fig. 2, CID experiments do not exclude energetically demanding fragmentation channels, making the direct formation of the aldehyde **3-H** possible.^{18a,c,d} Finally, the computed energetics in Fig. 2 show that the formation of the triplet state of **2-H_t** is thermodynamically unlikely, as its energy lies 53.6 kJ mol⁻¹ above the singlet ground state.⁸ Moreover, the process is kinetically inhibited due to the generally slow singlet to triplet intersystem crossing for molecules without heavy atoms. In line with this, no evidence of the hydroxycarbene triplet **2-H_t** appears in the IR spectrum of the ions at m/z 164 (see Supplementary Fig 3). A similar argument holds for CO-loss from **2-H_c**.

II.2 Isomerization kinetics of hydroxy[4-(trimethylammonio)phenyl]carbene (**2-H/2-D**) measured by isomer-selective infrared ion spectroscopy

Prior to the analysis of the isomerization kinetics, the deuterated isotopologue **1-D** was decarboxylated upon CID and the resulting product ions at m/z 165 were subjected to IR ion spectroscopy. The respective IR spectrum is in convincing agreement with the computed one of **2-D**, but also delivers evidence for the concomitant presence of the aldehyde tautomer **3-D** on the basis of the clearly detected carbonyl stretching mode (see Supplementary Figure 6, SI).

To investigate the time-dependence of the isomerization of the hydroxycarbenes **2-H_t** and **2-D_t** to their respective aldehydes **3-H** and **3-D**, IR photodissociation experiments were completed placing a delay (0-20 s) between generation of m/z 164/165 by CID and probing by IR photodissociation. Fig. 3 displays the normalized

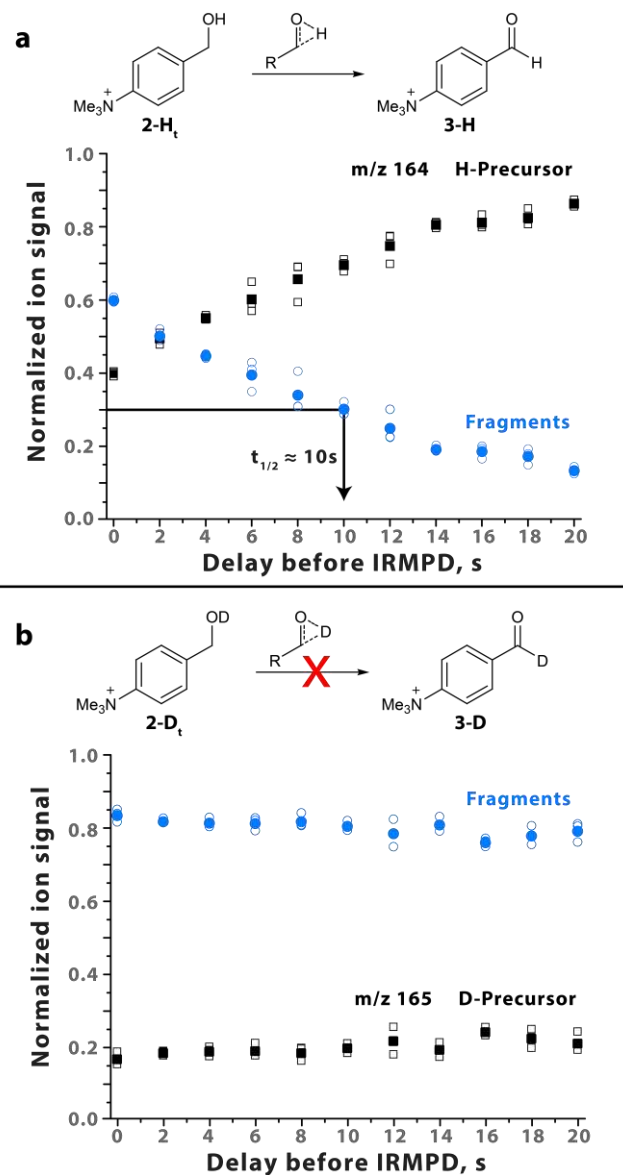


Figure 3. Time-dependent IRMPD measurements of deuterated and non-deuterated m/z 164/165 ions. Hydroxycarbene-selective photodissociation yields were measured at 1300 cm⁻¹ where hydroxycarbene species are resonant and give fragmentation, and aldehyde species are transparent and not detected. Black squares represent the normalized precursor ion signal and blue circles represent the sum of the normalized fragment signals, which are shown in Supplementary Table 3 (IR yield). Three measurements were taken at each delay time (open symbols) and are averaged (closed symbols).

photofragment signal vs. the normalized precursor ion signal as a function of the delay. Using a wavelength of 1300 cm⁻¹, where **2-H_t** and **2-D_t** are both resonant, while cold **3-H** and **3-D** are transparent (see Fig. 1 and Supplementary Fig. 6), the isomerization of the hydroxycarbene species to aldehyde can be inferred from a decreasing photofragment signal with increasing delay. Panel (a) of Fig. 3 shows that the maximum fragment ion signal from m/z 164 is indeed observed at t=0 s and has

almost completely decayed after 20 s, indicating a loss of resonance at 1300 cm^{-1} due to isomerization to the transparent aldehyde species. Conversely, under the same conditions, m/z 165 shows essentially no decay in fragmentation signal over the full range of 20 s, indicating that no isomerization takes place and m/z 165 remains resonant with photons at 1300 cm^{-1} .

Together with the identification of the aldehyde **3-H** structure (see Fig. 1, above) as the minor component of the ion population at m/z 164 (see Fig. 3a at 0s), these results show that the decay of **2-H_t** is accompanied by the progressive formation of aldehyde **3-H**. This isomerization reaction of **2-H_t** to **3-H** and the absence of the corresponding isomerization of **2-D_t** to **3-D** represents a direct observation of hydrogen tunneling at room temperature and above.

Reaction mechanisms that do not involve tunneling imply small primary kinetic isotope effects (KIEs) for reactions where the hydrogen transfer proceeds via a non-linear TS, a criterion that clearly applies to the 1,2-H-shift in **2-H_t**, as Scheme 1 and Figs. 2 and 3 illustrate.²⁰ In contrast, large primary kinetic isotope effects ($\text{KIE}_{\text{H/D}} = k_{\text{H}} / k_{\text{D}}$) are found when tunneling is involved ($\text{KIE} > 6.4$ at 300 K)^{3,4,21} and competitive reaction isotope effects can be excluded.²²

Isomerization of hydroxycarbene **2-H_t** to aldehyde **3-H** occurs with a $t_{1/2}$ of approximately 10 s. In the case of the 1,2-H-shift in **2-H_t**, k_{D} is close to zero as the deuterated hydroxycarbene **2-D_t** does not appreciably isomerize over the time frame of the experiments (20 s), indicating a major primary KIE. A quantitative analysis of the data is presented in Supplementary Figs. 7 and 8 and suggests a $\text{KIE} > 20$. If **2-H_t** were to isomerize to **3-H** without involving tunneling, the Eyring equation shows that the KIE should be approximately 1.2 at 298 K based on the calculated Gibbs free energies of activation for **2-H_t** and **2-D_t**. We note that the substantially shorter half-life of about 9.5 ± 0.3 s in our experiments above room temperature (see Supplementary Figure 7, SI), compared to 2.5 h at 11 K determined by Schreiner et al.^{8,23} for phenylhydroxycarbene, suggests a reduced effective barrier width for the isomerization. This must be due to the elevated temperature, given that the computed barriers for the neutral phenylhydroxycarbene and the charge tagged derivative investigated here are similar. The elevated temperature (and associated vibrational excitation) means that the height of the barrier is smaller relative to the internal energy of the molecule and that the barrier is narrower (see Supplementary Fig. 13).⁸ In addition, lower-energy vibrational modes will be more extensively populated in our experiment compared to the one by Schreiner. Taken together, this may lead to a lower barrier due to geometric and/or electronic changes in the molecule, whereby the anharmonicity of those low-energy vibrations is likely to play a role as well.

Based on the large KIE observed for the gas-phase isomerization reaction of **2-H_t** to **3-H**, we conclude that the 1,2-H shift reaction of the hydroxycarbene **2-H_t** probed at temperatures above RT can dominantly be attributed to hydrogen tunneling.^{3,24} It shall finally be mentioned that studies of Gronert²⁴ and O’Hair²⁵ suggest that ions stored in spherical QITs at RT at a He pressure of about $\sim 10^{-3}$ mbar, are quickly (in milliseconds)²⁶ and effectively cooled by numerous collisions with the He buffer gas, and ultimately thermalize to an effective temperature of about 320-350 K.^{18a,18b} At a T_{eff} of 350 K thermal isomerization is virtually impossible for **2-H_t**, due to the substantial energy barrier of about 128 kJ mol^{-1} , providing further support for the assumption that the observed isomerization of hydroxycarbene **2-H_t** to **3-H** proceeds via hydrogen tunneling.

III. Conclusions

In summary, we present the first spectroscopic evidence for hydrogen tunneling at temperatures above 300K using two-color tautomer selective vibrational spectroscopy of gaseous, isolated molecular ions. A charge-tagged phenylhydroxycarbene was generated by the decarboxylation of oxo[4-(trimethylammonio)phenyl]acetic acid in an ion trap mass spectrometer and its structure and reactivity probed by infrared ion spectroscopy using an infrared free electron laser (FELIX) in combination with quantum chemical modelling.¹⁵ The hydroxycarbene undergoes 1,2-H-shift to its corresponding aldehyde, which can be clearly distinguished by isomer-selective two-color infrared-infrared depletion experiments. The deuterated carbene analogue shows negligible 1,2-D-shift reactivity, providing clear evidence that the hydrogen atom rearrangement proceeds via tunneling. This observation is the first spectroscopic confirmation of hydrogen tunneling at non-cryogenic temperatures and provides a firm basis for the interpretation of tunneling-controlled processes such as enzymatic reactivity³⁻⁵ and organocatalysis.²⁷⁻²⁹ Additionally, these results open up new avenues for further investigation of the intrinsic reactivity of hydroxycarbenes at room temperature in ion trap mass spectrometers via ion molecule reactions.^{11,30}

EXPERIMENTAL SECTION

Mass spectrometry

The compounds **1-H**, **1-D**, **3-H** and **3-D** were freshly synthesized for this study (see Supporting Information for details) and characterized by positive ion mode electrospray ionization mass spectrometry ((+)ESI-MS).^{18b} Compounds **1-H** and **3-H** were dissolved ($c \sim 10^{-5}$ M) in CH_3OH , compounds **1-D**, **3-D** were analyzed in $\text{CD}_3\text{OD}/\text{CH}_3\text{OH}$. All (+)ESI-MS and MS^2 experiments as well as accurate ion mass measurements were conducted on an LTQ-Orbitrap XL instrument (Ther-

moFisher, Bremen Germany); see Supplementary Figures 1 and 2. Product ion spectra were acquired in the linear ion trap (LTQ) part of the LTQ-Orbitrap instrument by CID with the He bath gas present ($P = 2 \times 10^{-5}$ Torr) and the product ions were analyzed in the orbitrap (see Supplementary Figure 2). Accurate ion masses were determined in the orbitrap analyser with a resolution of 30000 FWHM with external calibration ($\Delta m < 3$ ppm) or with addition of internal standards ($\Delta m < 2$ ppm). Typical (+)ESI-MS conditions: Flow rate: $5 \mu\text{L min}^{-1}$; Capillary voltage: 3.20 kV; Sheath gas: 4.99 [arb. units]; Aux gas: 2.00 [arb. units]; Resolution: 30000 FWHM.

Infrared ion spectroscopy

A modified spherical 3D quadrupole ion trap mass spectrometer (Bruker, Amazon Speed ETD) was used for the infrared ion spectroscopy experiments and has been described in detail elsewhere.¹³ The 3D quadrupole ion trap was operated at ambient temperature (~ 320 K) with a He pressure in the trap of $\sim 10^{-3}$ mbar to assure optimal performance (e.g. effective collisional cooling, signal to noise ratio, sensitivity etc.).¹³ Tunable radiation for the photodissociation experiments was generated by the Free Electron Laser for Infrared eXperiments (FELIX)^{13,15,16} in the $600 - 1800 \text{ cm}^{-1}$ range and a pulsed OPO (LaserVision, USA) source in the $2800 - 3700 \text{ cm}^{-1}$ range both operating at a repetition frequency of 10 Hz. Pulse energies were approximately 20 – 50 mJ per 5 μs long macropulse for the FEL and 10 – 20 mJ per 5 ns long pulse for the OPO. The full width at half maximum bandwidth of the FEL is approximately 0.4% of the central wavelength and 3 cm^{-1} for the OPO. Precursor ions were formed by electrospray ionization from solutions of $0.5 \mu\text{M}$ in methanol at a flow rate of $120 \mu\text{L hr}^{-1}$. Ions were irradiated for 1 s, corresponding to interaction with 10 laser pulses. The IR spectra were constructed from a series of mass spectra recorded with the laser scanning over the frequency range from $600 - 1800 \text{ cm}^{-1}$, monitoring the intensity of the IR-induced product ions (primarily methyl radical loss) and the depletion of the precursor ion as a function of IR frequency. Unimolecular dissociation results from the absorption of multiple IR photons (IRMPD). The IR yield ($\Sigma I_{\text{fragment ions}} / \Sigma I_{\text{all ions}}$) was determined after laser irradiation at each frequency and was linearly corrected for frequency-dependent variations in laser power. A grating spectrometer (wavemeter) was used to calibrate the absolute frequency of the FEL (OPO).

Time-dependent measurements of the isomerization reaction by selective IR photodissociation

Four steps were used for these experiments: 1) Isolation and CID fragmentation of the precursor ions at m/z 208 (**1-H**) and m/z 209 (**1-D**), respectively, to induce CO_2 loss and product ion formation at m/z 164 or 165, respectively. 2) Isolation of the CID product ions at m/z

164 (mixture of carbene **2-H** and aldehyde **3-H** of unknown ratio) from **1-H** and analogously at m/z 165 from **1-D**. 3) Variable delay of 0 to 20 s. 4) IRMPD at 1300 cm^{-1} of m/z 164 or m/z 165 ions for 1 s. 11 Data points (each an average of four mass spectra) were triply measured for these time-dependent measurements by increasing the delay in steps of 2 s. The dissociation yield (normalized total fragment ion intensity = IR yield) for the non-deuterated species decreases from approximately 0.6 at $t = 0$ s, to approximately 0.14 at $t = 20$ s. For the deuterated species, the IR yield is nearly constant over the full range of delay times. We note that the difference in the dissociation yields between the non-deuterated/deuterated species at 1300 cm^{-1} in their respective IR spectra corresponds closely to the difference in yields measured here at $t = 0$ s. The dissociation yield at 1300 cm^{-1} is taken as a diagnostic for the fraction of m/z 164 ions being in the carbene isomeric form (compare experimental spectra in Fig. 1a and 1b).

Two color IR-IR isomer selective infrared ion spectroscopy

The first laser set at a fixed frequency dissociates all ions resonant at that selected frequency, here 3553 cm^{-1} . A 10 W cw-OPO (Argos 2400 BB) was used as the “burn”-laser. A second, tunable laser is then used to record the IR spectrum of the remaining ions (those that were transparent to the frequency of the first laser), in an analogous manner as the single laser experiments described above. Specifically, CID product ions at m/z 164 (unknown mixture of carbene **2-H_t** and aldehyde **3-H**) were generated from the m/z 208 precursor ion. We note that after decarboxylation, the ions are collisionally cooled before IR irradiation (10’s of ms separation between these steps).^{18,26} After isolation of m/z 164, the ions were irradiated for 40 ms with the output from the cw-OPO tuned to the carbene OH stretch at 3553 cm^{-1} , which depletes all ions in the trap absorbing at this frequency, i.e. having a hydroxycarbene structure. The aldehyde **3-H** isomer has no resonances near this frequency and remains unaffected. After 40 ms, further depletion of the m/z 164 signal was not observed, indicating that all hydroxycarbene ions were removed from the population. The remaining ions at m/z 164 (those transparent at 3553 cm^{-1}) were again mass-isolated and held in the trap for 1 s while being irradiated by the FEL, which was tuned point-by-point over the $800 - 1800 \text{ cm}^{-1}$ region. Thus, an isomer-selective IR spectrum was obtained.

A two-color IR-IR approach was also used to selectively measure the IR spectrum of the fragmentation product of the hydroxycarbene **2-H_t** species resulting from $\cdot\text{CH}_3$ loss (m/z 149). As described in the IR-IR scheme above, CID product ions at m/z 164 (mixture of carbene **2-H_t** and aldehyde **3-H**) were isolated and irradiated at 3553 cm^{-1} by the cw-OPO. This selectively induces dissociation of the carbene species, but not of

the aldehyde species. In the next step, rather than isolate the remaining ions at m/z 164 (which are assumed to be aldehyde **3-H**), the fragment ions from the hydroxycarbene **2-H_t** at m/z 149 were instead mass-isolated. An IRMPD spectrum was then recorded using the FEL selectively for this $^{\bullet}\text{CH}_3$ -loss product of the carbene species.

Computations

Density functional theory (DFT) calculations were performed using Gaussian09, version D.01.³¹ Gaussian was compiled with Gaussian-supplied versions of BLAS and ATLAS.³² The B3LYP³² functional was used throughout this study with the GD3-BJ correction³⁴ to account for dispersion interactions, whereby it is noted that in this case the correction did not significantly affect the results in comparison to the bare B3LYP functional. The cc-pVTZ basis³⁵ set was used throughout with the ultrafine setting for the integrals. This computational procedure is an improvement on the procedure from our earlier work, which already gave a good correlation with experiments.^{36–38} All the calculations performed on these systems were done in vacuo. Intrinsic reaction coordinate (IRC) calculations were performed with the calculation of frequencies at every step of the profile. The calculation of the barrier penetration integral was done using the IRC profile following the procedure used by Schreiner et al. outlined in their supporting information,⁸ using atomic units throughout. CCSD(T)-F12b³⁹ calculations were carried out with the MOLPRO package of ab initio programs,⁴⁰ using the cc-pVDZ-F12 basis set⁴¹ along with matching auxiliary fitting bases.⁴² The geminal Slater exponent was set to $1.0 a_0^{-1}$.

ASSOCIATED CONTENT

Supporting Information

Experimental details of the synthesis of the carbene precursors and reference aldehydes. Cartesian coordinates and energies of all calculated structures, zero-point corrected energy profile of the carbene formation and the isomerization to the respective aldehyde. Additional Figures, Tables, and X-ray data of 4-(trimethylammonio)benzaldehyde (**3-H**) and of [4-(Dimethylamino)-phenyl]oxo(O-²H)acetic acid (**S-2-D**).

AUTHOR INFORMATION

Corresponding Author

Correspondence and requests for materials should be addressed to M.S. (mathias.schaefer@uni-koeln.de), A.B. (berkessel@uni-koeln.de), J.O. (j.oomens@science.ru.nl), and A.J.H.M.M. (a.meijer@sheffield.ac.uk).

Funding Sources

No competing financial interests have been declared. Funding from the European Community's Seventh Framework Programme (FP7/2007–2013) under grant agreement n.°312284, and by the Fonds der Chemischen Industrie is gratefully acknowledged.

ACKNOWLEDGMENT

The authors thank Professor Stefan Schlemmer, Institute of Physics, University of Cologne and Professor Frank Tu-recek, University of Washington, Seattle, USA for critical discussion of the experiments and results, Dr. Jörg Neudörfel, Department of Chemistry, University of Cologne, for x-ray crystallography, BSc Thomas Thomulka for synthesizing 1-H, and BSc Rianne van Outersterp for assistance with the time-dependent IR measurements. We wish to thank Dr. J. Grant Hill of the University of Sheffield for his help in running the CCSD(T) calculations. The skillful assistance of the entire FELIX staff is gratefully acknowledged. A license for the OpenEye tools, obtained via the free academic licensing program, is gratefully acknowledged.

REFERENCES

- (1) Bell, R. P. *The Tunnel Effect in Chemistry*, Chapman & Hall: New York, USA, **1980**.
- (2) (a) McMahon, R. J. *Science* **2003**, 299, 833–834. (b) Borden, W. T. *WIREs Comput. Mol. Sci.* **2016**, 6, 20–46. (c) Kästner, J. *WIREs Comp. Mol. Sci.* **2014**, 4, 158–168.
- (3) Bothma, J. P.; Gilmore, J. B.; McKenzie, R. H.; *New J. Phys.* **2010**, 12, 055002.
- (4) (a) Roston, D.; Islam, Z.; Kohen, A. *Molecules* **2013**, 18, 5543–5567. (b) Kohen, A.; Cannio, R.; Bartolucci, S.; Klinman, J. P. *Nature* **1999**, 399, 496–499.
- (5) Meisner, J., Kästner, J. *Angew. Chem. Int. Ed.* **2016**, 55, 5400–5413.
- (6) Schreiner, P. R.; Reisenauer, H. P.; Pickard IV, F. C.; Simmonett, A.C.; Allen, W. D.; Mátyus, E.; Császár, A. G. *Nature* **2008**, 453, 906–909.
- (7) Schreiner, P. R.; Reisenauer, R. P.; Ley, D.; Gerbig, D.; Wu, C.-H.; D. Allen, W. D. *Science* **2011**, 332, 1300–1303.
- (8) Gerbig, D.; Reisenauer, H.P.; Wu, C.H.; Ley, D.; Allen, W.D.; Schreiner, P. R. *J. Am. Chem. Soc.* **2010**, 132, 7273–7275.
- (9) Bucher, G. *Angew. Chem. Int. Ed.* **2008**, 47, 6957–6958.
- (10) Zuev, P. S.; Sheridan, R. S.; Albu, T. V.; Truhlar, D. G.; Hrovat, D. A.; Borden W. T. *Science* **2003**, 299, 867–870.
- (11) O’Hair, R. A.; Rijs, N. J. *Acc. Chem. Res.* **2015**, 48, 329–340.
- (12) (a) Jordan, F.; Patel, H. *ACS Catal.* **2013**, 3, 1601–1617. (b) Breslow, R. *Acc. Chem. Res.* **1995**, 28, 146–153. (c) Frank, R. A. W.; Leeper, F. J.; Luisi, B. F. *Cell. Mol. Life Sci.* **2007**, 64, 892–905.
- (13) (a) Martens, J.; Grzetic, J.; Berden, G.; Oomens, J. *Nat. Commun.* **2016**, 7, 11754. (b) Martens, J.; Berden, G.; Gebhardt, C.R.; Oomens, J. *Rev. Sci. Instrum.* **2016**, 87, 103108.
- (14) Gross, M.L.; *Charge-Remote Fragmentation: Applications and Mechanism*. In *The Encyclopedia of Mass Spectrometry*; Gross, M.L.; Caprioli, R.; Eds. Elsevier: Amsterdam, **2005**, Vol 4, pp. 361–370.
- (15) (a) Polfer, N. C. *Chem. Soc. Rev.* **2011**, 40, 2211–2221. (b) Polfer, N. C.; Oomens, J. *Mass Spectrom. Rev.* **2009**, 28, 468–494. (c) Roithova, J. *Chem. Soc. Rev.* **2012**, 41, 547–559.
- (16) Martens, J. K.; Grzetic, J.; Berden, G.; Oomens, J. *Int. J. Mass Spectrom.* **2015**, 377, 179–187.
- (17) So, S.; Kirk, B. B.; Trevitt, A. J.; Wille, U.; Blanksby, S.J.; da Silva, G. *Phys. Chem. Chem. Phys.*, **2014**, 16, 24954–24964.
- (18) (a) McLuckey, S. A.; Goeringer, D. E. *J. Mass Spectrom.* **1997**, 32, 461–474. (b) Gabelica, V.; De Pauw, E. *Mass Spectrom. Rev.* **2005**, 24, 566–587. (c) March, R. E. *J. Mass Spectrom.* **1997**, 32, 351–369. (d) March, R. E. *Ion Traps*. In *The Encyclopedia of Mass Spectrometry*; Gross, M.E.; Caprioli, R. Eds. Elsevier: Amsterdam, **2004**, Vol 1, pp. 144–158.
- (19) Zuev, P. S.; Sheridan, R. S.; Albu, T. V.; Truhlar, D. G.; Hrovat, D. A.; Borden, W. T. *Science*, **2003**, 299, 867–870.
- (20) Anslyn, E. V.; Dougherty, D. A. *Modern Physical Organic Chemistry*, University Science Books: Sausalito, USA **2006**.

- (21) Kim, Y.; Kreevoy, M. M. *J. Am. Chem. Soc.* **1992**, *114*, 7116-7123.
- (22) Osterheld, T. H.; Braman, J. I. *J. Am. Chem. Soc.* **1992**, *114*, 7158-7164.
- (23) Ley, D.; Gerbig, D.; Wagner, J. P.; Reisenauer, H. P.; Schreiner, P. R. *J. Am. Chem. Soc.* **2011**, *133*, 13614-13621.
- (24) Derkits, D.; Wiseman, A.; Snead, R. F.; Dows, M.; Harge, J.; Lamp, J. A.; Gronert, S. *J. Am. Soc. Mass Spectrom.* **2016**, *27*, 339-343.
- (25) Donald, W. A.; Khairallah, G. N.; O'Hair, R. A. *J. Am. Soc. Mass Spectrom.* **2013**, *24*, 811-815.
- (26) Pepin, R.; Tureček, F. *J. Phys. Chem. B* **2015**, *119*, 2818-2826.
- (27) Enders, D.; Niemeier, O.; Henseler, A. *Chem. Rev.* **2007**, *107*, 5606-5655.
- (28) Hopkinson, M. N.; Richter, C.; Schedler, M.; Glorius, F. *Nature* **2014**, *510*, 485-496.
- (29) Flanigan, D. M.; Romanov-Michailidis, F.; White, N. A.; Rovis, T. *Chem. Rev.* **2015**, *115*, 9307-9387.
- (30) (a) O'Hair, R. A. *J. Int. J. Mass Spectrom.* **2015**, *377*, 121-129. (b) Fiebig, L.; Schlörer, N.; Schmalz, H.-G.; Schäfer, M. *Chem. Eur. J.* **2014**, *20*, 4906-4910. (c) Fiebig, L.; Kuttner, J.; Hilt, G.; Schwarzer, M. C.; Frenking, G.; Schmalz, H.-G.; Schäfer, M. *J. Org. Chem.* **2013**, *78*, 10485-10493. (d) Vikse, K. L.; McIndoe, J. S. *Pure Appl. Chem.* **2015**, *87*, 361-377.
- (31) Frisch, M. J.; Trucks, G. W.; Schlegel, H. B.; Scuseria, G. E.; Robb, M. A.; Cheeseman, J. R.; Scalmani, G.; Barone, V.; Mennucci, B.; Petersson, G. A.; Nakatsuji, H.; Caricato, M.; Li, X.; Hratchian, H. P.; Izmaylov, A. F.; Bloino, J.; Zheng, G.; Sonnenberg, J. L.; Hada, M.; Ehara, M.; Toyota, K.; Fukuda, R.; Hasegawa, J.; Ishida, M.; Nakajima, T.; Honda, Y.; Kitao, O.; Nakai, H.; Vreven, T.; Montgomery, J. A., Jr.; Peralta, J. E.; Ogliaro, F.; Bearpark, M.; Heyd, J. J.; Brothers, E.; Kudin, K. N.; Staroverov, V. N.; Kobayashi, R.; Normand, J.; Raghavachari, K.; Rendell, A.; Burant, J. C.; Iyengar, S. S.; Tomasi, J.; Cossi, M.; Rega, N.; Millam, J. M.; Klene, M.; Knox, J. E.; Cross, J. B.; Bakken, V.; Adamo, C.; Jaramillo, J.; Gomperts, R.; Stratmann, R. E.; Yazyev, O.; Austin, A. J.; Cammi, R.; Pomelli, C.; Ochterski, J. W.; Martin, R. L.; Morokuma, K.; Zakrzewski, V. G.; Voth, G. A.; Salvador, P.; Dannenberg, J. J.; Dapprich, S.; Daniels, A. D.; Farkas, Ö.; Foresman, J. B.; Ortiz, J. V.; Cioslowski, J.; Fox, D. J. *Gaussian v. 09*, Gaussian, Inc., Wallingford, CT, **2009**.
- (31) (a) Whaley, R. C.; Petitet, A. *Software Pract. Exper.* **2005**, *35*, 101-121. (b) Whaley, R. C.; Petitet, A.; Dongarra, J. J. *Parallel Comput.* **2001**, *27*, 3-35.
- (33) Becke, A. D. *J. Chem. Phys.* **1993**, *98*, 5648-5652.
- (34) Grimme, S.; Ehrlich, S.; Goerigk, L. *J. Comput. Chem.* **2011**, *32*, 1456-1465.
- (35) Kendall, R. A.; Dunning, T. H.; Harrison, R. J. *J. Chem. Phys.* **1992**, *96*, 6796-6806.
- (36) Holland, M. C.; Berden, G.; Oomens, J.; Meijer, A. J. H. M.; Schäfer, M.; Gilmour, R. *Eur. J. Org. Chem.* **2014**, *26*, 5675-5680.
- (37) Massah, A. R.; Dreiocker, F.; Jackson, R. F. W.; Pickup, B. T.; Oomens, J.; Meijer, A. J. H. M.; Schäfer, M. *Phys. Chem. Chem. Phys.* **2011**, *13*, 13255-13267.
- (38) Ross, A. J.; Dreiocker, F.; Schäfer, M.; Oomens, J.; Meijer, A. J. H. M.; Pickup, B. T.; Jackson, R. F. W. *J. Org. Chem.* **2011**, *76*, 1727-1734.
- (39) Knizia, G.; Adler, T. B.; Werner, H.-J. *J. Chem. Phys.* **2009**, *130*, 054104.
- (40) (a) Werner, H.-J.; Knowles, P. J.; Knizia, G.; Manby, F. R.; Schütz, M.; Celani, P.; Korona, T.; Lindh, R.; Mitrushenkov, A.; Rauhut, G.; Shamasundar, K. R.; Adler, T. B.; Amos, R. D.; Bernhardsson, A.; Berning, A.; Cooper, D. L.; Deegan, M. J. O.; Dobbyn, A. J.; Eckert, F.; Goll, E.; Hampel, C.; Hesselmann, A.; Hetzer, G.; Hrenar, T.; Jansen, G.; Köppl, C.; Liu, Y.; Lloyd, A. W.; Mata, R. A.; May, A. J.; McNicholas, S. J.; Meyer, W.; Mura, M. E.; Nicklass, A.; O'Neill, D. P.; Palmieri, P.; Peng, D.; Pflüger, K.; Pitzer, R.; Reiher, M.; Shiozaki, T.; Stoll, H.; Stone, A. J.; Tarroni, R.; Thorsteinsson, T.; Wang, M. *MOLPRO, a package of ab initio programs, v. 2012.1*, **2012**. (b) Werner, H. J.; Knowles, P. J.; Knizia, G.; Manby, F. R.; Schütz, M. *WIREs Comput. Mol. Sci.* **2012**, *2*, 242-253.
- (41) Peterson, K. A.; Adler, T. B.; Werner, H.-J. *J. Chem. Phys.* **2008**, *128*, 084102-1-12.
- (42) (a) Weigend, F. A. *Phys. Chem. Chem. Phys.* **2002**, *4*, 4285-4291. (b) Yousaf, K. E.; Peterson, K. A. *J. Chem. Phys.* **2008**, *129*, 184108. (c) Kritikou, S.; Hill, J. G. *J. Chem. Theory Comput.* **2015**, *11*, 5269-5276.

Table of Contents graphics:

